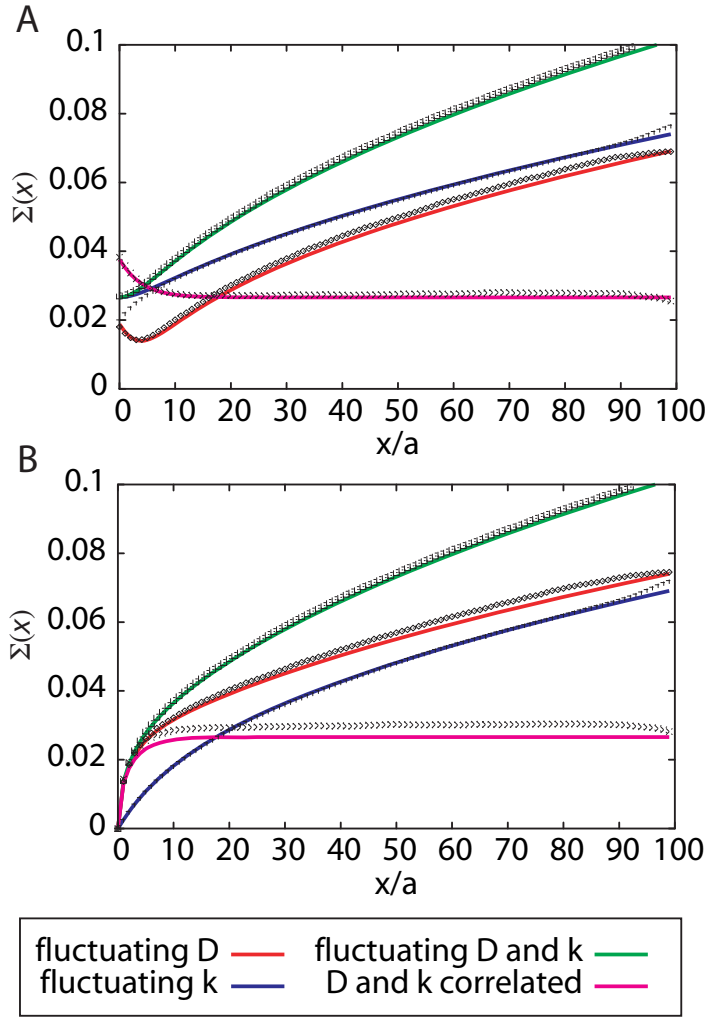

Fig. S1. Relative uncertainty Σ(*x*) of the steady state concentration *c(x)* for the diffusion-degradation model with disorder in one dimension (1). (**A**,**B**) The symbols indicate results from numerical calculations in which steady-state gradients were calculated for many (typically 100,000) realizations of the disorder. The lines show the corresponding analytical results (8) for Σ(*x*). The red lines show Σ(*x*) if only *D* is fluctuating, the blue lines if only *k* is fluctuating, the green lines if both *D* and *k* are fluctuating, and the magenta lines if *D* and *k* are fluctuating in a fully correlated way. In A, the current *j* is imposed at *x*=0. In B, the concentration *c* is imposed at *x*=0. Parameters are $\lambda / a = \sqrt{50}$, $\sigma_j / j_0 = \sigma_{c_0} / c_0 = 0$, $\sigma_D / D_0 = \sigma_k / k_0 = 0.1$. In the fully correlated case $2\rho_{kD} / k_0 D_0 = (\sigma_D / D_0)^2 + (\sigma_k / k_0)^2$ while ρ_{kD}=0 otherwise. A Gaussian distribution was used for the noise terms in the numerical calculations. Steady states were calculated on a linear chain of size 100*a*.

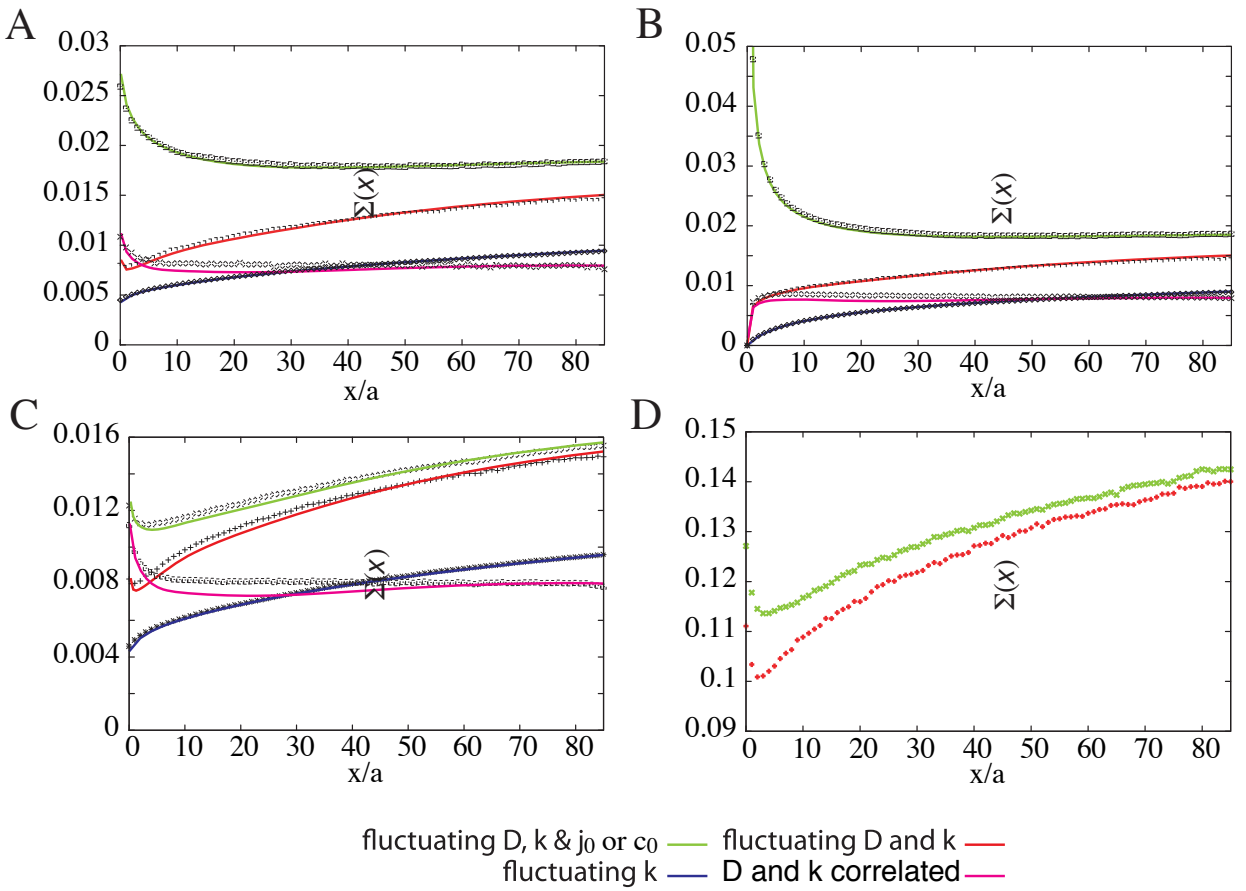

Fig. S2. Relative uncertainty Σ(*x*) of the steady state concentration *c(x)* for the diffusion-degradation model with disorder in two dimensions. The symbols indicate results from numerical calculations in which steady-state gradients were calculated for many (typically 100,000) realizations of the disorder. The lines show the corresponding analytical results for Σ(*x*) that follow from (10). The blue lines show Σ(*x*) if only *k* is fluctuating, the red lines if both *D* and *k* are fluctuating, the magenta line if *D* and *k* are fluctuating in a fully correlated way, and the green lines if *D*, *k* and the respective quantity imposed at the boundary at $x=0$ (j or c_0) are fluctuating. (**A**) Relative concentration uncertainty Σ(*x*) with the current *j* imposed at $x=0$. (**B**) Σ(*x*) with the concentration c_0 imposed at $x=0$. (**C**) Like A, but with parameters corresponding to Fig. 2 of the main manuscript. (**D**) Relative concentration uncertainty Σ(*x*) for the general case in which the hopping rates between two neighboring sites in opposite direction are uncorrelated. Current *j* imposed at $x=0$. Compared to A-C, the magnitude of Σ(*x*) is increased in this situation. Parameters as in Fig. S1, with $\sigma_j / j_0 = \sigma_{c_0} / c_0 = 0.1$ in A,B, $\sigma_j / j_0 = 0.037$ in C, $\sigma_j / j_0 = 0.25$ in D, and $\lambda / a = 7$ in C,D. A Gaussian distribution was used for the noise terms in the numerical calculations. Steady states were calculated on a simple cubic lattice of size $100a \times 100a$.

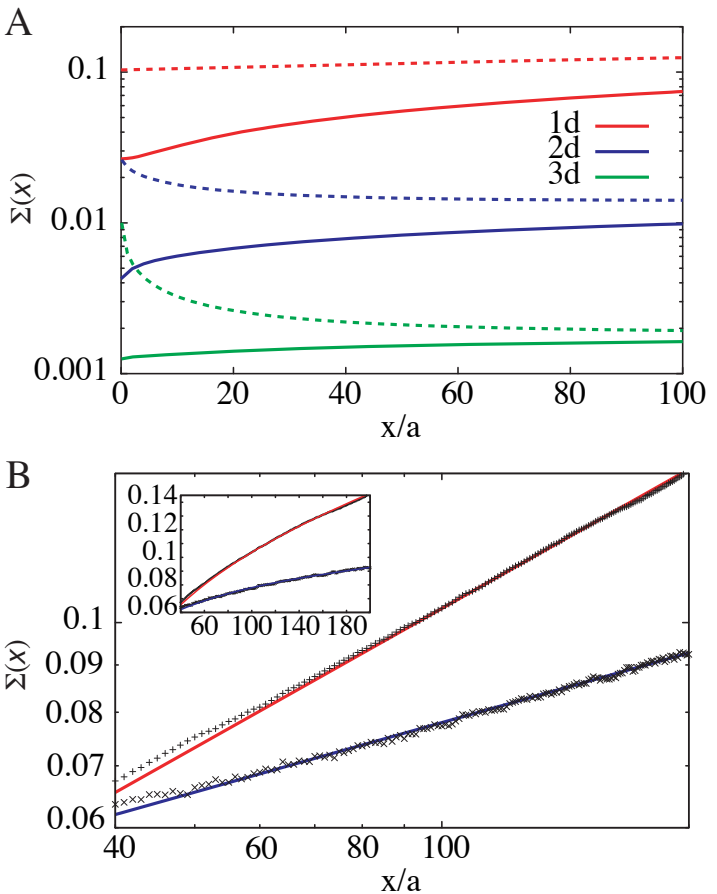

Fig. S3. Relative concentration uncertainty $\Sigma(x)$ for the diffusion-degradation model with disorder for different space dimensionalities. All calculations were done with j imposed at x=0. (**A**) Logarithmic plot of $\Sigma(x)$ in one dimension (red lines), in two dimensions (blue lines), and in three dimensions (green lines). For the solid lines, only k is fluctuating and for the broken lines both k and j are fluctuating. Shown are the analytical results for $\Sigma(x)$ given by (8), (10) and (12) for the different space dimensionalities respectively. (**B**) Double-logarithmic plot of $\Sigma(x)$ for large x in one and two dimensions. In these calculations, k and D are fluctuating. Numerical results are shown by symbols. In two dimensions, $\Sigma(x)$ was multiplied by a factor of five. For comparison, functions proportional to $x^{1/2}$ and $x^{1/4}$ are shown in red and blue, respectively. The inset shows the same data using linear axes. Parameters as in Fig. S1 with $\sigma_j / j_0 = 0.1$ and $\rho_{kD} = 0$. Steady states in two dimensions were calculated on a simple cubic lattice of size $220a \times 100a$.

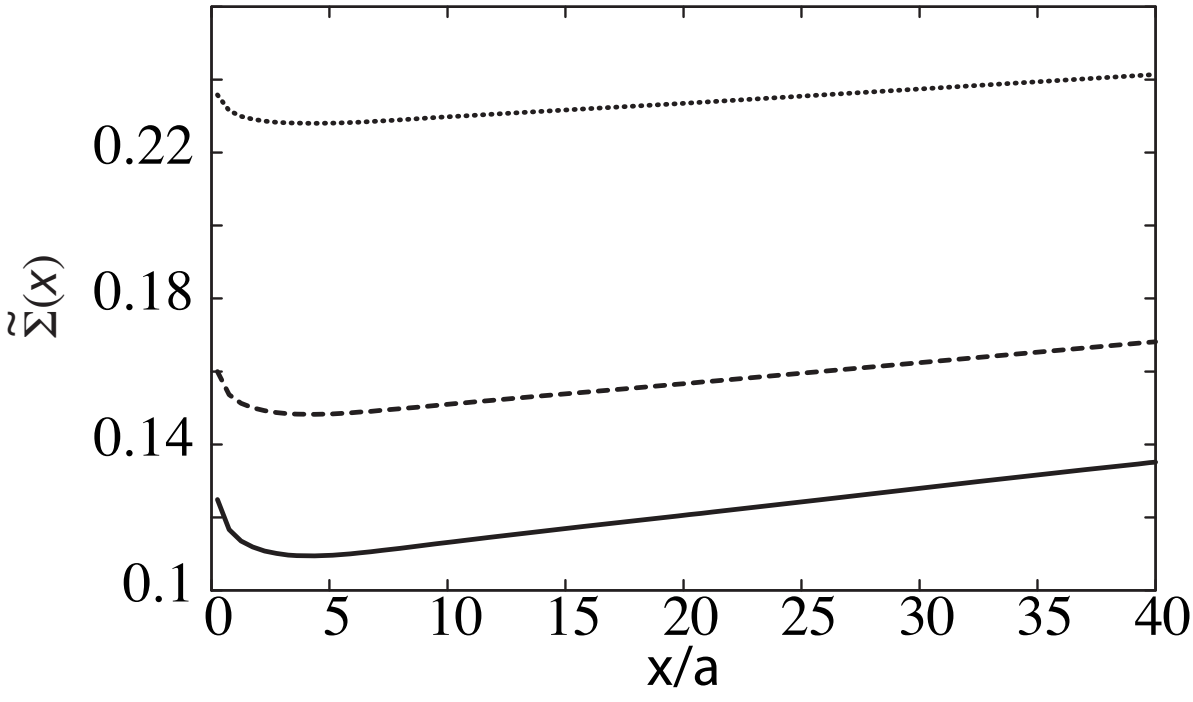

Fig. S4. Relative concentration uncertainty $\tilde{\Sigma}(x)$ in presence of disk-to-disk variations of the current imposed at x=0. For the solid line $\sigma_{j_0} / j_0^0 = 0$, for the dashed line $\sigma_{j_0} / j_0^0 = 0.1$, and for the dotted line $\sigma_{j_0} / j_0^0 = 0.2$. Remaining parameters as in Fig. 2 of the main manuscript.

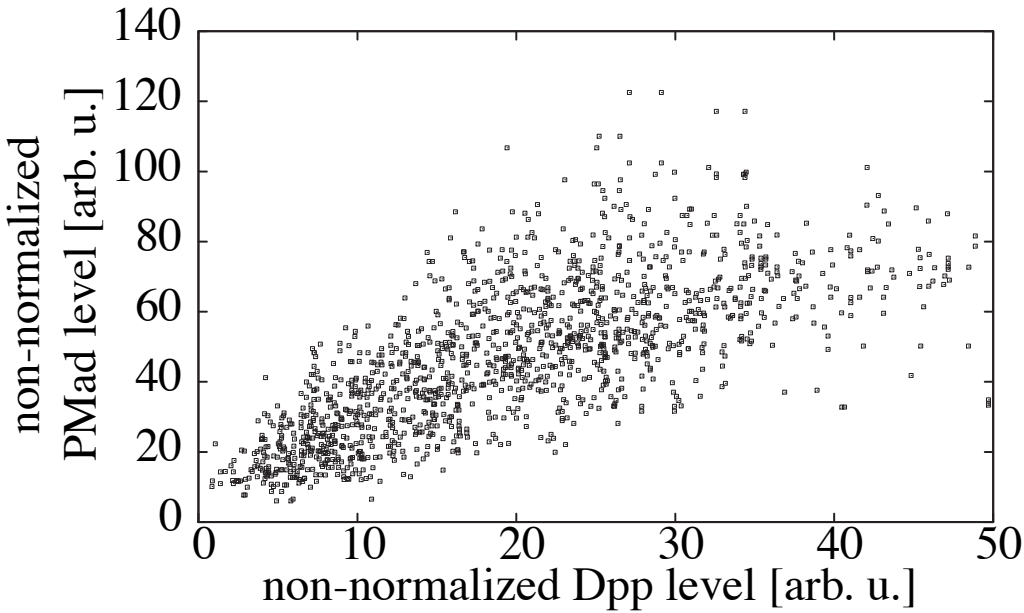

Fig. S5. Correlations between PMad and Dpp concentrations. Non-normalized PMad level of all nuclei shown in Fig. 5B of the main manuscript correlated with the non-normalized GFP-Dpp level at the same distance from the source in the same wing disk (R=0.63). Compare with Fig. 5C of the main manuscript, which shows the same plot for the normalized PMad data. These data were obtained from a set of N=15 wing disks from *dpp* mutants rescued by a GFP-Dpp transgene using the UAS/Gal4 driver system.

I. THEORETICAL DESCRIPTION OF MORPHOGEN TRANSPORT IN A TISSUE WITH CELL-TO-CELL VARIABILITY

We introduce cell-to-cell variability as random components to the diffusion coefficient and the degradation rate in the diffusion-degradation equation which describes the time evolution of the morphogen concentration profile, see equation (1) in the experimental procedure of the main manuscript. This is done most naturally in a discrete description. We consider a lattice with sites corresponding to individual cells. In one dimension, the morphogen concentration on site n is denoted C_n, with $n = 0, 1, 2, \ldots$. Molecules are transported to neighboring sites with rates p_n^+ (from site n to $n+1$) and p_n^- (for the transport from $n+1$ to n). In addition, molecules on site n are degraded with a rate k_n. Cell-to-cell variability leads to variations of the rates $p_n^\pm$ and k_n as a function of n. To keep our discussion simple, we restrict ourselves to the simpler situation where $p_n = p_n^+ = p_n^-$, i.e. transport in opposite directions between cells occurs at the same rate p_n.

The concentrations C_n satisfy the kinetic equation

$$\partial_t C_n = p_{n-1}(C_{n-1} - C_n) + p_n(C_{n+1} - C_n) - k_n C_n, \quad \text{for } n > 0, \tag{1}$$

where $\partial_t = \partial/\partial t$. The lattice begins at site $n = 0$ corresponding to the morphogen source. Two different boundary conditions are considered: fixed concentration C_0^0 and a morphogen source at $n = 0$ emitting morphogens at an imposed rate ν. The concentration C_0 then satisfies

$$\partial_t C_0 = \nu + p_0(C_1 - C_0) - k_0 C_0. \tag{2}$$

This discrete description can be generalized to square (or cubic) lattices in two and three dimensions (see Fig. 3 of the main manuscript).

In the absence of disorder (cell-to-cell variability) $p = p_n$ and $k = k_n$ are the same for all sites. On large scales, the concentrations follow a diffusion-degradation equation $\partial_t c = D\nabla^2 c - kc$ with $D = pa^2$ and degradation rate k. Here, $c(x) = C_n$ with $x = an$. Cell-to-cell variability corresponds to a situation where $p_n = p + \eta_n$ and $k_n = k + \zeta_n$. Here, η_n and ζ_n are random variables with zero average. They are characterized by their correlators which we choose to be $\langle \eta_n \eta_j \rangle = \sigma_D^2/a^4 \delta_{nj}$ and $\langle \zeta_n \zeta_j \rangle = \sigma_k^2 \delta_{nj}$. Here, the brackets $\langle \ldots \rangle$ denote an ensemble average over all realizations of the random variables. These relations imply that the values of η_n and ζ_n at different bonds of the lattice are uncorrelated. The η_n and ζ_n can

also be correlated at each lattice site: $\langle \eta_n \zeta_j \rangle = \rho_{kD}/a^2 \delta_{nj}$.

In addition to the rates p_n and k_n, the rate of ligand influx into the system ν can be fluctuating, i.e. $\nu = \nu_0 + \chi$ where χ is a random variable with $\langle \chi \rangle = 0$, $\langle \chi^2 \rangle = \sigma_j^2/a^2$, and $\langle \chi \eta_n \rangle = \langle \chi \zeta_n \rangle = 0$ for all $n \geq 0$. In the case of a fixed concentration at $n = 0$, one can introduce fluctuations at the boundary very similarly: $C_0 = C_0^0 + \gamma$ with a random variable γ satisfying $\langle \gamma \rangle = 0$, $\langle \gamma^2 \rangle = \sigma_{c_0}^2$, and $\langle \gamma \eta_n \rangle = \langle \gamma \zeta_n \rangle = 0$. The standard deviations σ_D/a^2, σ_k, σ_j/a, and σ_{c_0} of the noise terms η_n, ζ_n, χ, and γ are assumed to be small compared to the mean values p, k, ν_0, and C_0^0 respectively. Our discussion is mostly independent of the specific probability distributions of η_n, ζ_n, χ, and γ. It is only required that these distributions are tightly localized around their mean value zero.

II. CONTINUUM LIMIT

In the presence of disorder, the kinetics of the concentration field can be described on large scales in a continuum limit. In d dimensions, with $\vec{x}$ describing a position in space, i.e. $\vec{x} = (x, y)$ in $d = 2$ and $\vec{x} = (x, y, z)$ in $d = 3$, the concentration field $c(t, \vec{x})$ obeys

$$\partial_t c(t, \vec{x}) = \nabla \cdot \left[(D_0 + \eta(\vec{x})) \nabla c(t, \vec{x}) \right] - (k_0 + \zeta(\vec{x})) c(t, \vec{x}) \tag{3}$$

Here $\eta(\vec{x})$ and $\zeta(\vec{x})$ denote noise terms with zero average and correlators $\langle \eta(\vec{x}) \eta(\vec{x}') \rangle = \sigma_D^2 a^d \delta(\vec{x} - \vec{x}')$, $\langle \zeta(\vec{x}) \zeta(\vec{x}') \rangle = \sigma_k^2 a^d \delta(\vec{x} - \vec{x}')$, and $\langle \eta(\vec{x}) \zeta(\vec{x}') \rangle = \rho_{kD} a^d \delta(\vec{x} - \vec{x}')$. These correlators express the continuum limits of the expressions introduced in the discrete case. The amplitude of the fluctuations of D is σ_D and accordingly σ_k for k. A possible correlation of the fluctuations of D and k at a given position is measured by ρ_{kD}.

The fluctuations of the secretion rate of the source cells located at $x < 0$ are captured by imposing a current

$$(D_0 + \eta(\vec{x})) \, \partial_x c(\vec{x}, t) \Big|_{x=0} = -j_0 - \chi(\vec{x}) \Big|_{x=0} \tag{4}$$

across the boundary surface at $x = 0$, where $\chi(\vec{x})$ is a noise term with $\langle \chi(\vec{x}) \chi(\vec{x}') |_{x=0} \rangle = \sigma_j^2 a^{(d-1)} \delta^{(d-1)}(\vec{x} - \vec{x}')|_{x=0}$.

A. Effects of disorder on steady state gradients

The steady state solutions $c(\vec{x})$ of (3) depend on the particular realization of the disorder, reflecting the effects of cell-to-cell variability. The average gradient $\bar{c}(x) = \langle c(\vec{x}) \rangle$ is given by

an ensemble average over all possible realizations of the disorder. Alternatively, in a two-dimensional geometry with a line source at $x = 0$, the average gradient can be determined by averaging along the y direction for given x in a single realization of the disorder.

We first discuss the problem in $d = 1$. It is assumed that the amplitude of the noise is small, i.e. $\sigma_D/D_0 \ll 1$ and $\sigma_k/k_0 \ll 1$. We calculate the variance of the concentration

$$\sigma_c^2(x) = \langle (c(x) - \bar{c}(x))^2 \rangle \tag{5}$$

by using a perturbation expansion to first order in the small parameters σ_D/D_0 and σ_k/k_0. Note that to first order the average concentration is given by $\bar{c}(x) = c_0 e^{-x/\lambda}$ where $\lambda = \sqrt{D_0/k_0}$ is the diffusion length and $c_0 = j_0/\sqrt{k_0 D_0}$.

The results of this calculation can be expressed in terms of Green's functions $G(x, x')$ of the linear operator $(D_0\partial_x^2 - k_0)$ which satisfy $(D_0\partial_x^2 - k_0)G(x, x') = \delta(x - x')$. To satisfy the two different boundary conditions at $x = 0$, two Green's functions $G_\pm(x, x')$ with $G_-(0, x') = 0$ and $\partial_x G_+(x, x')|_{x=0} = 0$ respectively are needed. In one dimension these functions are given by

$$G_\pm(x, x') = \frac{-1}{2\sqrt{k_0 D_0}} \left(e^{-|x-x'|/\lambda} \pm e^{-(x+x')/\lambda} \right). \tag{6}$$

To first order in our perturbation expansion, the variance of the concentration is given by

$$\begin{aligned} \langle \sigma_c^\pm(x)^2 \rangle \;=\; & D_0^2 \left(\partial_{x'} G_\pm(x, x') \Big|_{x'=0} \right)^2 \sigma_{c_0}^2 + G_\pm(x, 0)^2 \sigma_j^2 \\ & + a \int_0^\infty dx' \Big(\sigma_D^2 \bar{c}'(x')^2 (\partial_{x'} G_\pm(x, x'))^2 + \sigma_k^2 G_\pm(x, x')^2 \bar{c}(x')^2 \\ & + 2\rho_{kD} G_\pm(x, x') \bar{c}(x') \bar{c}'(x') \partial_{x'} G_\pm(x, x') \Big). \end{aligned} \tag{7}$$

Here, we use a condensed notation for both choices of the boundary condition at $x = 0$: σ_c^+ denotes the solution for a fixed current and σ_c^- the solution for a fixed concentration at $x = 0$. Using the explicit expressions for the Green's functions and $\bar{c}(x)$, this integral can be solved and expressed in terms of elementary functions. As discussed in the main text, a dimensionless measure of the relative concentration uncertainty at x is

$$\Sigma(x) = \frac{\left\langle (c(x) - \bar{c}(x))^2 \right\rangle^{1/2}}{\bar{c}(x)} = \frac{\langle \sigma_c(x)^2 \rangle^{1/2}}{\bar{c}(x)}.$$

Using (7), one obtains to first order in perturbation theory

$$\Sigma^\pm(x) \;=\; \left(\Sigma_B^\pm(x)^2 + \Sigma_k^\pm(x)^2 + \Sigma_D^\pm(x)^2 + \Sigma_{kD}^\pm(x) \right)^{1/2}, \text{ with}$$

$$
\begin{aligned}
\Sigma_B^+(x)^2 &= \left(\frac{\sigma_j}{j_0}\right)^2 \\
\Sigma_B^-(x)^2 &= \left(\frac{\sigma_{c_0}}{c_0}\right)^2 \\
\Sigma_k^\pm(x)^2 &= \frac{a}{8\lambda}\left(\frac{\sigma_k}{k_0}\right)^2\left(1 \pm 2 \mp e^{-2x/\lambda} + \frac{2x}{\lambda}\right) \\
\Sigma_D^\pm(x)^2 &= \frac{a}{8\lambda}\left(\frac{\sigma_D}{D_0}\right)^2\left(1 \mp 2 \pm 3e^{-2x/\lambda} + \frac{2x}{\lambda}\right) \\
\Sigma_{kD}^\pm(x) &= \frac{a}{4\lambda}\frac{\rho_{kD}}{k_0 D_0}\left(1 \pm e^{-2x/\lambda} - \frac{2x}{\lambda}\right). \qquad (8)
\end{aligned}
$$

As the relative concentration fluctuations become arbitrarily large for large x, these results are only valid in a finite region $0 \le x \le M$ for some $M > 0$.

The steady state of (3) for $d = 2$ can be calculated iteratively as in the one dimensional situation. The free Green's function for the operator $(D_0(\partial_x^2 + \partial_y^2) - k_0)$ satisfying $(D_0(\partial_x^2 + \partial_y^2) - k_0)G_0(\vec{x}, \vec{x}') = \delta(\vec{x} - \vec{x}')$ is

$$G_0(\vec{x}, \vec{x}') = \frac{-1}{2\pi D_0} K_0(|\vec{x} - \vec{x}'|/\lambda),$$

where K_0 is a modified Bessel function of the second kind [1]. Using a mirror image technique, one can construct Green's functions $G_\pm(\vec{x}, \vec{x}')$ that satisfy $G_-(\vec{x}, \vec{x}')|_{x=0} = 0$ and $\partial_x G_+(\vec{x}, \vec{x}')|_{x=0} = 0$ respectively:

$$G_\pm(x, y, x', y') = G_0(x, y, x', y') \pm G_0(x, y, -x', y'). \qquad (9)$$

To first order, the variance of $c(\vec{x})$ is

$$
\begin{aligned}
\langle \sigma_c^\pm(\vec{x})^2 \rangle &= a\int_{-\infty}^{\infty} dy' \left(\sigma_{c_0}^2 D_0^2 \left(\partial_{x'} G_\pm(\vec{x}, \vec{x}')\Big|_{x'=0}\right)^2 + \sigma_j^2 G_\pm(x, y, 0, y')^2\right) \\
&\quad + a^2 \int_0^\infty dx' \int_{-\infty}^{\infty} dy' \Big(\sigma_k^2 G_\pm(\vec{x}, \vec{x}')^2 \bar{c}(x')^2 + \sigma_D^2 \bar{c}'(x')^2 (\partial_{x'} G_\pm(\vec{x}, \vec{x}'))^2 \\
&\quad + 2\rho_{kD} \bar{c}(x') \bar{c}'(x') G_\pm(\vec{x}, \vec{x}') \partial_{x'} G_\pm(\vec{x}, \vec{x}')\Big). \qquad (10)
\end{aligned}
$$

The resulting relative concentration uncertainty grows asymptotically as $\Sigma(x) = \langle \sigma_c(\vec{x})^2 \rangle^{1/2} / \bar{c}(x) \sim x^{1/4}$. The first term in (10) is due to the fluctuations of the current across the boundary line at $x = 0$ or the concentration that is fixed there. This term alone decreases as $\Sigma(x) \sim x^{-1/4}$ for large x. Positive correlations between the fluctuations of k_0 and D_0 increase the precision as in the one dimensional case.

One can calculate the standard deviation of the concentration in $d = 3$ as well. We are interested in the steady state solution of (3) with $\vec{x} = (x, y, z)$ and $\nabla = (\partial_x, \partial_y, \partial_z)$ in the

half-space $x \geq 0$. Either the concentration or the current is imposed on the boundary plane $x = 0$, i.e. $c(\vec{x})|_{x=0} = c_0 + \gamma(y, z)$ or $\partial_x c(\vec{x})|_{x=0} = -D_0^{-1}(j_0 + \chi(y, z))$.

The Green's functions for the two boundary conditions at $x = 0$ can again be constructed:

$$G_\pm(\vec{x}, \vec{x}') = \frac{-1}{4\pi D_0}\left(\frac{e^{-r/\lambda}}{r} \pm \frac{e^{-r_m/\lambda}}{r_m}\right), \tag{11}$$

with $r = ((x - x')^2 + (y - y')^2 + (z - z')^2)^{1/2}$ and $r_m = ((x + x')^2 + (y - y')^2 + (z - z')^2)^{1/2}$. The result for the variance of $c(\vec{x})$ to first order in perturbation theory is

$$\begin{aligned}\langle \sigma_c^\pm(\vec{x})^2 \rangle \;=\; & a^2 \int_{-\infty}^{\infty} dy' \int_{-\infty}^{\infty} dz' \left(\sigma_{c_0}^2 D_0^2 \left(\partial_{x'} G_\pm(\vec{x}, \vec{x}')\right)^2 + \sigma_j^2 G_\pm(\vec{x}, \vec{x}')^2\right)\Big|_{x'=0} \\ & + a^3 \int_0^{\infty} dx' \int_{-\infty}^{\infty} dy' \int_{-\infty}^{\infty} dz' \Big(\sigma_k^2 G_\pm(\vec{x}, \vec{x}')^2 \bar{c}(x')^2 + \sigma_D^2 \bar{c}'(x')^2 (\partial_{x'} G_\pm(\vec{x}, \vec{x}'))^2 \\ & + 2\rho_{kD} \bar{c}(x') \bar{c}'(x') G_\pm(\vec{x}, \vec{x}') (\partial_{x'} G_\pm(\vec{x}, \vec{x}'))\Big).\end{aligned} \tag{12}$$

We have integrated (12) numerically. The resulting relative concentration uncertainty $\Sigma(x)$ is shown in Suppl. Fig. 3 A for a fixed current at the boundary. Asymptotically, $\Sigma(x) \sim \ln(x)$. The contribution from the boundary term alone decreases asymptotically as $\Sigma(x) \sim x^{-1/2}$.

B. Effects of disk-to-disk variations of the morphogen secretion rate

As discussed in the main text, the total fluorescence intensity (FI) of the non-normalized GFP-Dpp FI profiles measured experimentally varies considerably from disk-to-disk. This is most likely due to variations in the secretion rate of morphogens from the source cells between wing disks from different larvae.

Such disk-to-disk variations can easily be included in our theoretical description. In addition to the cell-to-cell fluctuations which are already taken into account in (4), we assume that the current imposed at $x = 0$ fluctuates with a standard deviation σ_{j_0} about its mean value j_0^0 for different gradients in our ensemble. We further assume that these fluctuations are not correlated with any of the cell-to-cell fluctuations in the system. The relative concentration uncertainty $\tilde{\Sigma}(x)$ that takes disk-to-disk variations of the morphogen secretion rate into account is then

$$\tilde{\Sigma}(x) = \sqrt{(\sigma_{j_0}/j_0^0)^2 + \Sigma(x)^2}, \tag{13}$$

where $\Sigma(x)$ is the relative concentration uncertainty in the absence of disk-to-disk variations of the morphogen secretion rate which was calculated above. In Suppl. Fig. 4, we show

$\tilde{\Sigma}(x)$ for different values of σ_{j_0}. While the behavior of $\tilde{\Sigma}(x)$ is qualitatively the same as that of $\Sigma(x)$, the minimum of $\tilde{\Sigma}(x)$ is less and less pronounced in relative terms for increasing values of σ_{j_0}.

III. NUMERICAL SIMULATIONS

We have performed numerical calculations of the discrete description (1) for the two different boundary conditions at $x = 0$ in one and two dimensions. At the remaining boundaries, we imposed zero flux boundary conditions. A large number of steady state gradients was calculated for different realizations of the disorder using a Gaussian distribution for the random variables. From these, the average value and standard deviation of C_n at all lattice sites n were calculated. The resulting relative concentration uncertainty is shown in Suppl. Fig. 1 for the different boundary conditions in $d = 1$ and in Suppl. Fig. 2 for $d = 2$. A good agreement with the results of the perturbative calculation is found.

Furthermore, we have numerically calculated the relative concentration uncertainty $\Sigma(x)$ in the general case in which the rates of transfer in opposite directions between neighboring sites are uncorrelated. In one dimension this implies $p_n^+ \neq p_n^-$ (Fig. 1C of the main manuscript). Suppl. Fig. 2D shows that while the qualitative features of $\Sigma(x)$ remain the same in this situation, the uncertainty is about an order of magnitude larger than in the case $p_n^+ = p_n^-$ for the same noise amplitude $\sigma_D/D_0 = 0.1$. This implies that the values of $\Sigma(x)$ are comparable to those observed experimentally.

---

[1] E. Weisstein, *Mathworld*, http://mathworld.wolfram.com/, wolfram Research, Inc.

Table S1. Average values and variability of the key quantities discussed in the main text

Quantity	Mean value [μm]	Standard deviation [μm]	Variation coefficient
GFP-Dpp decay length λ^{Dpp}	17.0	4.3	0.26
PMad decay length λ^{PMad}	25.2	4.5	0.18
Sal range x^*	39.1	6.1	0.16
Wing disk size L	132.6	21.0	0.16

These results were obtained from a set of N=15 wing disks from *dpp* mutants rescued by a GFP-Dpp transgene using the UAS/Gal4 driver system.

Table S2. Correlation indices *R* of the key quantities discussed in the main text

	λ^{Dpp}	λ^{PMad}	x^*	L	I^{Dpp}
λ^{PMad}	–0.04				
x^*	0.39	0.49			
L	0.14	0.03	0.56		
I^{Dpp}	0.13	0.30	0.26	–0.22	
I^{PMad}	0.18	0.33	0.58	0.55	0.29

The strongest correlations are observed between the disk size L and Sal range x^*, the total PMad level I^{PMad} and x^* and between I^{PMad} and L. These results were obtained from a set of N=15 wing disks from *dpp* mutants rescued by a GFP-Dpp transgene using the UAS/Gal4 driver system.